Brueckner, Gammel, and Kubis[16] (BGK), who also used the BGT potential. Our results for $\mathcal{E}^{(0,1)}$ always lie lower than their prediction for E/N. The magnitude of the discrepancy is about 25% at the lowest density ($r_0=3.0$ F) and increases monotonically with density to about 40% of the BGK value at $r_0=1.5$ F, corresponding to the highest density for which comparison can be made. Thus, under the more realistic nucleon-nucleon potentials, the results of $\mathcal{E}^{(0,1)}$ again show that the neutron system does not have a bound state.

In closing, it should be emphasized that the work on the neutron gas reported here is of a preliminary and exploratory nature. A great deal of work remains to be done, namely, the accurate calculation of $\mathcal{E}^{(0,1)}+\mathcal{E}^{(0,2)}$ for the neutron system with realistic two-neutron interactions. $\mathcal{E}^{(0,2)}$ here is an energy-correction term in zeroth cluster, and second perturbative order. Notable deficiencies of the present study involve neglect of noncentral components of the potentials and adoption of a simple correlation factor $f(r)$ too simple to satisfy certain physical boundary conditions.[18,19] It is our immediate goal to eliminate or minimize these deficiencies.

ACKNOWLEDGMENT

I am deeply grateful to Professor John W. Clark for his invaluable advice and encouragement.

[18] J. W. Clark and T. P. Wang, Ann. Phys. (N.Y.) **40**, 127 (1966).

[19] E. Feenberg, in *Lectures in Theoretical Physics*, Edited by W. E. Brittin pp. 160–174. (University of Colorado Press, Boulder, Colo. 1965), Vol. VIIC; J. Math. Phys. **6**, 658 (1965).

PHYSICAL REVIEW VOLUME 177, NUMBER 4 20 JANUARY 1969

Pion Capture in ^{6}Li and ^{7}Li, the Formation of ^{4}H, a Search for ^{5}H*

R. C. MINEHART, L. COULSON, W. F. GRUBB, III, AND K. ZIOCK
Department of Physics, University of Virginia, Charlottesville, Virginia

(Received 9 September 1968)

The breakup of ^{6}Li and ^{7}Li into two charged particles following π^- capture is studied. The branching ratios for the reactions $\pi^-+{}^6\text{Li}\rightarrow{}^2\text{H}$ (3.4×10^{-4}), $\pi^-+{}^7\text{Li}\rightarrow{}^3\text{H}+{}^4\text{H}$ (3.7×10^{-4}), and $\pi^-+{}^7\text{Li}\rightarrow{}^3\text{H}+{}^4\text{H}^*$ (4×10^{-4}) are measured. The energy of the ground state and first excited state (^{4}H*) of particle-unstable ^{4}H are found to be 2.9 and 6.1 MeV above the energy of the unbound ^{3}H+n. An upper limit is set for the branching ratio of the reaction $\pi^-+{}^7\text{Li}\rightarrow{}^2\text{H}+{}^5\text{H}$ ($<2\times10^{-4}$).

INTRODUCTION

NEGATIVE pions stopping in matter undergo nuclear capture. Upon capture the pion delivers its rest energy of 139.59 MeV to the capturing nucleus without transferring any linear momentum. Since capture on a single nucleon without significant excitation of the residual nucleus does not conserve energy and momentum, unless the capturing nucleon is in the high-momentum end of the nuclear Fermi distribution,[1] capture on a correlated pair of nucleons is the dominant capture mode in light nuclei.[2]

Besides this dominant mode there are others which, although much rarer, hold considerable interest. These modes lead to the fission of the capturing nucleus into two fragments of approximately equal mass. The existence of fission modes should enable one to study the importance of clusters in light nuclei. An even more attractive feature, and the one on which we have concentrated, is that the fission fragments may be short-lived nuclear systems that are difficult to form otherwise. Because of the large pion rest energy these fragments are produced with such kinetic energies that the method of missing mass spectrometry can be applied. It should also be noted at this point that, because the pion has isospin $T=1$, pion capture can lead to final states that are difficult to reach otherwise.

We have used this technique to study pion capture in ^{6}Li and ^{7}Li. Postulating only charge conservation, one expects that the following two-body breakup reactions might occur:

$\pi^-+{}^6\text{Li}\rightarrow{}^5\text{He}+n$	$\pi^-+{}^7\text{Li}\rightarrow{}^6\text{He}+n$
$\rightarrow{}^4\text{He}+{}^2n$	$\rightarrow{}^5\text{He}+{}^2n$
$\rightarrow{}^3\text{He}+{}^3n$	$\rightarrow{}^4\text{He}+{}^3n$
$\rightarrow{}^2\text{He}+{}^4n$	$\rightarrow{}^3\text{He}+{}^4n$
$\rightarrow{}^5\text{H}+{}^1\text{H}$	$\rightarrow{}^2\text{He}+{}^5n$
$\rightarrow{}^4\text{H}+{}^2\text{H}$	$\rightarrow{}^6\text{H}+{}^1\text{H}$
$\rightarrow{}^3\text{H}+{}^3\text{H},$	$\rightarrow{}^5\text{H}+{}^2\text{H}$
	$\rightarrow{}^4\text{H}+{}^3\text{H}.$

The notation ^2n, ^3n, etc., is used for the hypothetical dineutron, trineutron, etc. ^{2}He is the hypothetical di-

* Work performed under a research grant of the National Aeronautics and Space Administration.

[1] J. LeTourneux, Nucl. Phys. **81**, 665 (1966).

[2] M. E. Nordberg, Jr., K. F. Kinsey, and L. R. Burman, Phys. Rev. **165**, 1096 (1968).

proton.[3] Apart from some of the more outlandish possibilities, the following reactions seem to be the most interesting

$$\pi^-+{}^6\mathrm{Li}\rightarrow 2{}^3\mathrm{H}. \quad (1)$$

This reaction leads to two stable particles in the final state. From conservation of energy and momentum and from the known masses of the particles involved it follows that the two tritons must be collinear in the laboratory system and must each have a kinetic energy of 61.63 MeV. All this makes reaction (1) eminently suitable for the test and calibration of the equipment. There is, however, some intrinsic interest in reaction (1) that transcends this technical aspect. If an excited state of the triton exists, one should be able to observe it in the reaction

$$\pi^-+{}^6\mathrm{Li}\rightarrow {}^3\mathrm{H}+{}^3\mathrm{H}^*, \quad (1')$$

even if the excited triton $^3\mathrm{H}^*$ is particle-unstable.[4] The reactions

$$\pi^-+{}^6\mathrm{Li}\rightarrow {}^2\mathrm{H}+{}^4\mathrm{H} \quad (2)$$

and

$$\pi^-+{}^7\mathrm{Li}\rightarrow {}^3\mathrm{H}+{}^4\mathrm{H} \quad (3)$$

should allow one to observe the hydrogen isotope $^4\mathrm{H}$, whose possible existence has stimulated a large number of investigations.

Similarly, the formation of $^5\mathrm{H}$ might be observed in the reactions

$$\pi^-+{}^6\mathrm{Li}\rightarrow {}^5\mathrm{H}+p \quad (4)$$

and

$$\pi^-+{}^7\mathrm{Li}\rightarrow {}^5\mathrm{H}+{}^2\mathrm{H}. \quad (5)$$

There exists a rather copious literature about the nuclei $^4\mathrm{H}$ and $^5\mathrm{H}$, and we refer for general information and for literature references to the review articles by Lauritsen and Ajzenberg-Selove[5] and by Meyerhof and Tombrello.[6] At this point we mention only the work of Cohen *et al.*,[7] who first found reactions (1)–(3).

The part of our own work dealing with reaction (3) has already been reported briefly.[8]

In the following we shall report our search for the reactions (1), (3), and (5).

EXPERIMENTAL SETUP

The experimental arrangement is shown in Fig. 1. A low-energy (100-MeV) π^- beam from the 600-MeV synchrocyclotron at the NASA Space Radiation Effects Laboratory in Newport News, Va., was stopped in a lithium target of 60 mg/cm^2 with an area of 100 cm^2. The stopping rate was approximately 60 pions/g sec. Scintillation counters were used to select events consisting of a pion stopping in the target followed by the emission of two charged particles.

A $123\bar{4}$ coincidence indicated a pion stopping in the lithium target. A 567 coincidence was interpreted as a pair of charged particles emitted by the target and a $123\bar{4}567$ coincidence was used to trigger the sonic spark chambers Sp1–Sp4 and the range chamber. The amount of aluminum absorber in front of the range chamber was varied depending on the particular reaction under study.

The *sonic chambers* had a sensitive area of 18×18 in., a gap width of $\frac{3}{8}$ in. with 0.001-in. Al foil on both sides. The sound signals were picked up by four ceramic microphones of $\frac{1}{8}$-in. diam and $\frac{1}{2}$-in. length.

The clock rate was 2 MHz. The chambers were continuously flushed with commercial spark-chamber gas (90% Ne and 10% He, Linde). Extensive performance tests with cosmic rays as well as with the tritons from reaction (1) showed the sonic chambers to be highly reliable and capable of a spatial resolution of approximately 1 mm.

The *range chamber* had a sensitive area of 18×18 in. and a gap width of $\frac{3}{8}$ in. It was filled with He bubbled through ethyl alcohol at 0°C. The chamber consisted of 15 gaps, each with a 0.003-in. Al foil on both sides. Details of the design of the range chamber and the sonic chambers and of the performance tests carried out with them have been described elsewhere.[9,10]

Commercial modular electronic circuitry was used for the fast logic. The readout of the sonic chambers, the range chamber, and the time of flight was accomplished with a home-built system using commercially printed circuit cards.[11]

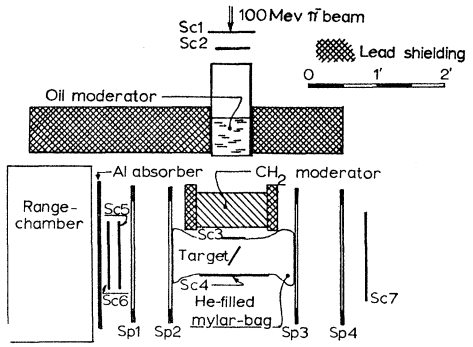

FIG. 1. Schematic view of the apparatus.

[3] Present experimental evidence and theoretical arguments strongly disfavor the existence of these hypothetical nuclei.

[4] We have reported elsewhere on an (unsuccessful) search for this reaction: L. Coulson, W. Grubb, R. Minehart, and K. Ziock (to be published).

[5] T. Lauritsen and F. Ajzenberg-Selove, Nucl. Phys. **78**, 1 (1966).

[6] W. A. Meyerhof and T. A. Tombrello, Nucl. Phys. **A109**, 1 (1968).

[7] R. C. Cohen, A. D. Kanaris, S. Margulies, and J. L. Rosen, Phys. Letters **14**, 242 (1965).

[8] K. Ziock, R. Minehart, L. Coulson, and W. Grubb, Phys. Rev. Letters **20**, 1386 (1968).

[9] L. Coulson, W. Grubb, R. Minehart, and K. Ziock, Nucl. Instr. Methods **61**, 209 (1968).

[10] W. Grubb, L. Coulson, R. Minehart, and K. Ziock (to be published).

[11] Flip Chips by Digital Equipment Corp.

EXPERIMENTAL PROCEDURE

For each event the following parameters were registered on punched paper tape: (a) the time elapsed between the spark and the response of the microphones in each of the four sonic chambers; (b) the penetration depth into the range chamber; and (c) the time of flight[12] between counters 3 and 5 and between counters 3 and 7. During the run a continuous check was kept on the performance of the range chamber. To this end the range of particles as given by indicator lights was written down and scrutinized for signs of malfunctions such as missing gaps, etc. The sonic chambers were checked occasionally for signs of accidental breakdowns. In the later analysis the only events accepted were those in which at least three sonic chambers had fired. This eliminated neutrons or γ rays converting in counters 5 or 7. The particle coordinates in the sonic spark chambers were computed and the particle trajectories were traced back to the target plane. For events originating in the target the angle between the two particle trajectories was computed.

CALIBRATION WITH REACTION (1) ($\pi^- + Li^6 \rightarrow 2H^3$)

This reaction, as mentioned above, provides a valuable means of testing the equipment. The tritons are monoenergetic and should give a peak in the range chamber whose width is determined only by the target thickness. The two tritons should, of course, have a strict 180° correlation, making their identification even easier. We searched for reaction (1) with a separated Li^6 target of 99% purity. Figure 2 shows the range distribution of all the charged particles originating in the target. The angular distribution of all target events

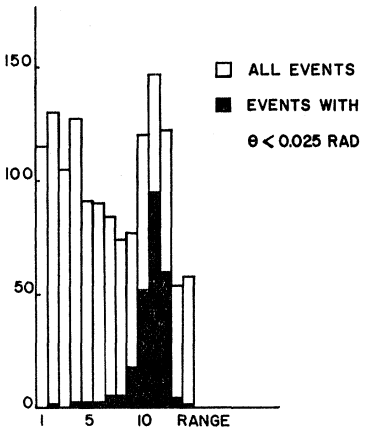

FIG. 2. Open histogram: range distribution of all charged-particle pairs from π^- capture in ^{6}Li. Solid histogram: range distribution of collinear pairs ($0<\theta<0.025$ rad).

[12] The time-of-flight resolution proved to be insufficient for the discrimination between protons and tritons and was not used in the analysis of our data.

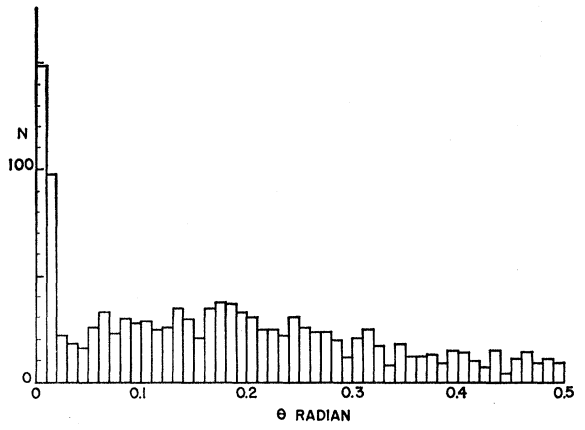

FIG. 3. Angular distribution of charged-particle pairs from π^- capture in ^{6}Li. The angle θ measures the deviation from collinearity. The plot includes only those pairs for which one particle stops in the range chamber.

is shown in Fig. 3, clearly indicating the presence of collinear events. The range of only the collinear particles is shown separately in Fig. 2, demonstrating that the peak seen in the raw data is indeed due to reaction (1).

DATA ANALYSIS

The analysis of the data was divided into the following steps: (a) reconstruction of the spark location in each of the four chambers; (b) computation of the geometry of the two-particle events; (c) determination of the range of the charged particle entering the range chamber; (d) distribution of the data according to range and angle between the two particles; and (e) statistical analysis. Each of these steps will now be discussed in detail.

Spark Location

The time between the breakdown of a sonic chamber and the detection of the sound by one of its microphones is related to the distances from the spark location to the microphone by

$$s = vt + r,$$

where r is an effective spark radius that accounts for the shock-wave region around the spark in which the velocity is large and varying. The distance s depends on the x and y Cartesian coordinates of the spark center, so that the above equation contains four parameters: x, y, v, and r. By measuring the time of the sound propagation to four different microphones all four parameters can be determined.

A symmetrical arrangement with all four microphones in the corners results in regions in the chamber where errors in microphone output are greatly amplified when converted to spark location. Breaking the symmetry by placing one microphone halfway between two corners eliminates this problem. However, the non-

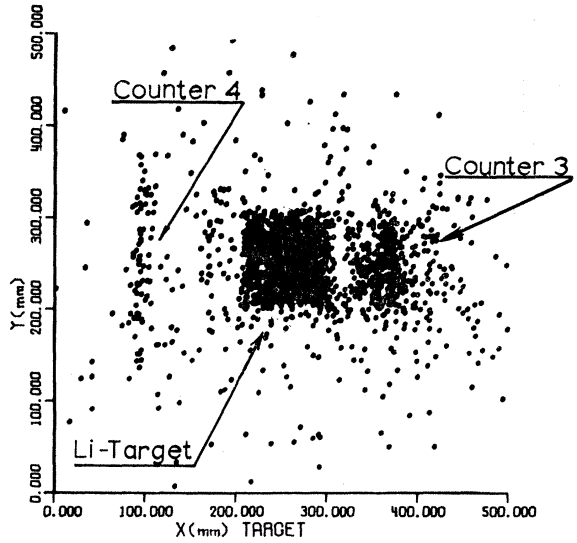

FIG. 4. Origin of events in the target plane.

symmetrical arrangement precludes an analytical solution for the four simultaneous equations and necessitates an iteration procedure to determine the spark coordinates.

In practice, the velocity of sound and the spark radius are sufficiently constant from event to event to assume predetermined values for these variables. It is then possible to solve analytically for x and y, thereby saving a substantial amount of computer time. The effect of this analysis procedure on the spark location for some arbitrarily selected events was found to be within the accuracy achieved by the iteration procedure.

Geometry

After locating each spark in the four sonic chambers, the two charged-particle trajectories were constructed. The distance of closest approach of the two trajectories was determined by constructing the minimum sphere tangent to both. The center of this sphere was taken to be the origin of the event. This method has a low accuracy for determining the intersection coordinate perpendicular to the plane of the chambers when the angle between the two trajectories is small. For those cases we located the intersections of the two trajectories with the target plane. The average of the two intersections was then taken as the origin of the event. If the separation between the two trajectories from the first method or the separation between intersection points obtained from the second method was greater than 1 cm, the event was discarded.

The accuracy of location of event origins is demonstrated in Fig. 4, which shows a plot of the points of origin projected onto the target plane. The target image is clearly visible in the plot, its edges are sharp, and its size agrees with the actual size of the target. Also visible are a dark line corresponding to the location of counter S3 and a fainter line corresponding to the location of the counter S4. Except for these regions of concentration the density outside the target area is low. Selection of events from the target region therefore results in a subset of the data with negligible nontarget background.

Range

The range chamber worked with high efficiency, so that 97% of the events resulted in the breakdown of a connected series of gaps, with the range determination being unambiguous. Consequently, the range could be determined simply from the last gap in a chain of firing gaps.

The angle between the particle trajectory and the normal to the absorber, as determined from the sonic-chamber coordinates, was used to compute the true range. The true range was expressed in terms of the range bin in which the particle would have stopped had it proceeded normally through the absorber. This correction shifted the two-triton range peak from ^{6}Li by 0.7 gaps. All the range curves shown in this paper have been corrected in this manner.

An effect of this correlation was to reduce the number of events in the first two gaps of the range chamber. Whereas many events were shifted out of these two gaps, there were none shifted into them from shorter ranges. We found that the correction removed 63% of the events from the first gap and 30% from the second gap. These percentages were determined by comparing the true range distribution with the uncorrected distribution of stopping points. Rather than discard the first two gaps, it was preferable to multiply the true range distribution by an appropriate depletion factor for each of the two gaps.

A correction was also made for the finite solid angle accepted by the range chamber. The location of the end point of the trajectory in the range chamber was calculated. We then required that the end point be inside the range chamber and at least 2 cm from any edge. With this criterion the solid angle accepted by the chamber is a function of the penetration depth. In calculating branching ratios this dependence of solid angle on penetration depth was taken into account.

Distributions

The next step in the analysis was the construction of a number of distributions. The data were separated into target or background events and distributed according to stopping point in the chamber and the angle between the two charged particles. To stop tritons of the appropriate energy it was necessary to insert some absorber between the range chamber and counter S6. Aluminum absorbers of 0.032- and 0.044-in. thickness were used. The difference of 0.012 in. equalled the amount of aluminum in two gaps of the range chamber. The distributions obtained with the two different absorbers

were compared and the locations of the two-triton peak from capture in the ^{6}Li differed indeed by two gaps.

After this test, the data from the two sets were added to form a total range curve with 16 bins. The data in the first and last two bins of this summed distribution come from only one of the two sets and were therefore normalized to the 12 bins in the overlap portion of the range curve.

SEARCH FOR ^{4}H

If ^{4}H is formed following pion capture in ^{7}Li, the range distribution of the tritons also formed in reaction (3) should show a peak. This peak is indeed exhibited by the 16-bin range distribution of the events from a natural Li target (92.6% ^{7}Li, 7.4% ^{6}Li) (Fig. 5) if one reduces the background from many-body breakups by

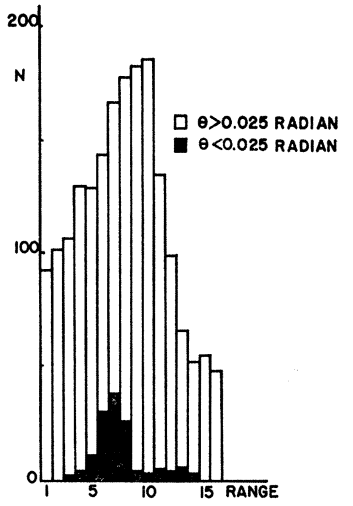

FIG. 5. Range distribution of events from π^- capture in natural Li. The solid histogram gives the range of the collinear events, attributed to π^- capture in the ^{6}Li content of the target.

including only events with an opening angle of less than 0.225 rad.[13] The angular distribution of *all* the charged-particle pairs whose one member stopped *inside* the range chamber is shown in Fig. 6.

If particle-stable ^{4}H were produced in our experiment, the two-charged particles would be collinear. In addition, collinear events from reaction (1) are expected from the ^{6}Li content of the target. Such collinear events appear indeed in Fig. 6, but their range distribution as shown separately in Fig. 5 identifies them by the location, magnitude, and width of the range peak as tritons from the reaction $\pi^-+{}^6\text{Li}\rightarrow 2^3\text{H}$ in the ^{6}Li content of the target. Thus it follows that our data show no evidence for a particle-stable ^{4}H. If particle-unstable ^{4}H decays into a triton and a neutron, the decay triton must fall within a cone surrounding the direction defined by the

[13] Upon insertion of an additional 0.012-in. Al absorber this peak also shifted properly, indicating that it was real and not caused by a malfunction of the range chamber.

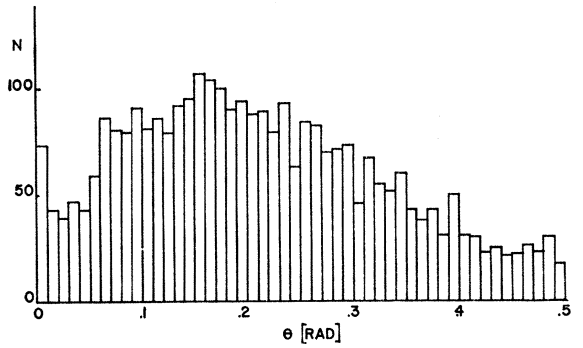

FIG. 6. Angular distribution of charged-particle pairs from π^- capture in natural Li. The plot includes only those pairs for which one particle stopped inside the range chamber. The angle θ measures the deviation from collinearity. The peak at $\theta=0$ is attributed to the reaction $\pi^-+{}^6\text{Li}\rightarrow 2^3$ H in the ^{6}Li content of the target.

first triton. The opening angle of this cone is, of course, determined by the energy available for the ^{4}H decay. The angular distribution within the cone can be easily calculated and Fig. 7 shows angular distributions calculated for various assumed parameters.

Information about the binding energy and the lifetime (level width) of ^{4}H is thus not only contained in the range distribution but also in the angular distribution of the events. We have, for this reason, distributed the ranges for various cuts in the angular distribution. These selected range distributions corresponding to 0.025-rad angular intervals are shown in Fig. 8, and show an important feature. For $\theta<0.125$ rad the peak is in gap 10. For each of the four angular intervals between $\theta>0.125$ and $\theta<0.225$ the peak is in gap 8. For

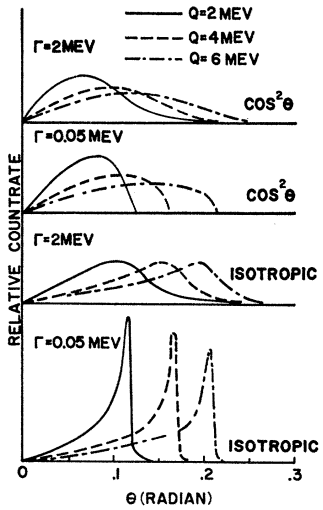

FIG. 7. Laboratory angular distributions for the two tritons from the reaction

$$\pi^-+{}^7\text{Li}\rightarrow{}^3\text{H}+{}^4\text{H}$$
$$\qquad\qquad\quad\ \ \lfloor\rightarrow{}^3\text{H}+n$$

for various assumed Q values, level widths, and angular distributions in the c.m. system.

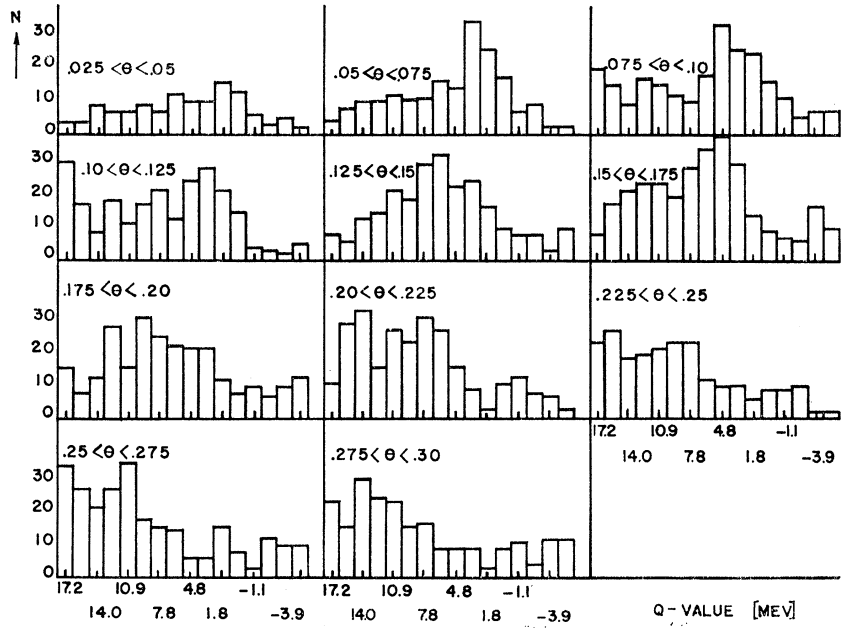

FIG. 8. Range distributions for various angular intervals.

$\theta > 0.225$ there may be evidence for a peak in the first few gaps of the range chamber. This shifting of the peak location indicates the existence of several energy levels of ^{4}H.

Note added in proof. To test our assumption that the two range peaks obtained for these two angular intervals are indeed due to the existence of two states of ^{4}H, a detailed statistical analysis was carried out. The results of this analysis, given in the next section, show that the angular and the energy distributions are indeed connected in the expected way.

With our assumption thus justified we have fitted three Gaussians and an exponential background to the range distributions for the two angular intervals $0.025 < \theta \leq 0.125$ rad and $0.125 \leq \theta \leq 0.225$ rad. This way of obtaining the energies and widths of the ^{4}H levels is inherently more accurate because an absolute energy calibration is provided by reaction (1). For reasons to be discussed later the evidence for a peak in the first few gaps of the chamber must be treated with considerable reservations. Consequently, we quote only results[13a] for two levels of ^{4}H as obtained from the range distribution fitting procedure:

(1) $E = 2.9$ MeV± 0.5 MeV,

$\Gamma = 3.0$ MeV± 1 MeV,

(2) $E = 6.1$ MeV± 0.5 MeV,

$\Gamma = 3.5$ MeV± 1 MeV.

The energies are referred to the energy of the unbound system ^{3}H$+n$. The numbers quoted here differ slightly (but well within statistical error) from those given in our letter[7] because of some refinements in the analysis.

Statistical Analysis

For a quantitative analysis the range distributions for each angular interval were fitted to a superposition of an (almost constant) exponential background and three Gaussians, corresponding to three discrete levels of the ^{4}H nucleus.[14] The centers of these Gaussians were varied independently for each angular cut and adjusted to obtain a best fit to the data. The results are summarized in Table I.

The essential features of the data shown in Table I are the following:

(a) The locations of the three Gaussians fitted independently for each angular range shift very little with angle.

(b) An appreciable number of events contributing to the first Gaussian occurs only at angles below 0.15 rad. A similar cutoff occurs for the second Gaussian at 0.25 rad.

Figure 9 shows the number of events under the first two Gaussians and their errors as given in Table I plotted as a function of angle. If the observed peaks in the *range* distributions (Fig. 8) do indeed represent different energy levels in ^{4}H, the *angular* distributions (Fig. 9) must fit theoretical distributions similar to the

[13a] To obtain the level widths, the finite target thickness and the resolution of the range chamber were taken into account.

[14] As mentioned above, there is a rise in the first few bins of our range distribution. If this rise is indeed due to a third energy level, the associated peak falls partly outside the energy range covered by our range chamber. For lack of more detailed knowledge we have accounted for this rise with a third Gaussian fitted to the range distributions. Since the two other peaks are well resolved, this third Gaussian affects their height and location very little.

TABLE I. Best-fit Gaussians. For each Gaussian the first column gives the location of the centroid in terms of the bin number in the corrected range distribution and the second column gives the area under the Gaussian and its statistical uncertainty in terms of the number of events represented by it. Column 8 gives the χ^2 for the fit with all three Gaussians. A χ^2 of 10 corresponds to a 50% probability. The widths assumed for the fits were $\sigma_1=\sigma_2=1.58$ MeV and $\sigma_3=2.24$ MeV.

	First Gaussian		Second Gaussian		Third Gaussian		
Angular interval[a] (rad)	Location of centroid (bin No.)	Area under Gaussian (No. of events)	Location of centroid (bin No.)	Area under Gaussian (No. of events)	Location of centroid (bin No.)	Area under Gaussian (No. of events)	χ^2
0.025–0.05	10.5	42±12	7.5	4±10	5	26±15	5.5
0.05–0.075	10.5	83±13	7.5	19±10	4	26±10	8.3
0.075–0.1	10.5	83±17	8.5	1±15	5	24±12	8.5
0.1–0.125	10	89±15	7.5	17±13	4	66±15	17.1
0.125–0.15	10	34±15	8.0	64±16	5	38±13	5.5
0.15–0.175	9.5	12±24	8.5	106±24	4	62±14	3.5
0.175–0.2	9.5	27±15	7.5	41±16	5	41±14	10.9
0.2–0.225	9.5	−28±11	7.5	94±14	3	61±15	15.7
0.225–0.25	10	−2±10	7.5	34±11	4	56±12	18.1
0.25–0.275	9.5	−10±8	8.0	20±13	4	82±14	25.1
0.275–0.3	10	−13±8	8.0	16±9	4	68±13	14.4

[a] Note that the first interval begins at 0.025 rad in order to exclude collinear events from pion capture in ^{6}Li.

ones given in Fig. 7 if the correct assumptions about the nature of the decay in the ^{4}H c.m. system are made. If the c.m. distribution of the angle between the decay triton and the laboratory momentum of the ^{4}H is known, the angular distribution in the lab frame can be calculated using the Q value of the decay (the difference between the mass of ^{4}H and the combined masses of ^{3}H and a neutron). Using Monte Carlo methods to incorporate the effects of the finite target thickness, the finite resolution of the range chamber, and the size and location of the detectors, we obtained laboratory distributions for isotropic and $\cos^2\theta$ c.m. distributions.

TABLE II. Least-squares fits to the distribution of decay angles for the first level of ^{4}H.

Q (MeV)	Γ (MeV)	χ^2 Isotropic decay	χ^2 $\cos^2\theta$ decay
3.4	2.5	35	9.0
3.4	3.0	34	7.6
3.4	3.5	43	8.3
3.4	4.0	39	6.3
3.2	2.5	29	7.7
3.2	3.0	31	6.3
3.2	3.5	27	12.9
3.2	4.0	33	8.3
3.0	2.5	34	7.2
3.0	3.0	23	9.5
3.0	3.5	28	7.9
3.0	4.0	31	9.3
2.8	2.5	23	8.9
2.8	3.0	24	7.0
2.8	3.5	24	10.1
2.8	4.0	27	8.2

These Monte Carlo distributions for several Q values and level widths of ^{4}H were then fitted by a least-squares process to the angular distributions shown in Fig. 9. The best fits and their parameters are included in the figure. The lowest level, or ground state, of ^{4}H could be fitted satisfactorily only by assuming either a $\cos^2\theta$ c.m. distribution or a triton energy that was at variance with the results of the range measurement. Since the triton energy corresponding to the center of the range peak can be determined to good accuracy as a

TABLE III. Least-squares fit to the distribution of decay angles for the second level of ^{4}H.

Q (MeV)	Γ (MeV)	χ^2 Isotropic decay	χ^2 $\cos^2\theta$ decay
7.5	2.0	19.5	56
7.5	2.5	21.2	54
7.5	3.0	21	60
7.5	3.5	23	62
7.5	4.0	23	56
7.3	2.0	18	...
7.3	2.5	19	59
7.3	3.0	22	60
7.3	3.5	20	60
7.3	4.0	22	61
7.1	2.0	18	...
7.1	2.5	16	59
7.1	3.0	18	61
7.1	3.5	25	65
7.1	4.0	21	65
6.9	2.0	21	63
6.9	2.5	19	61
6.9	3.0	20	68
6.9	3.5	26	65

TABLE IV. Branching ratios for two-particle break-up reactions.

	Reaction		
	$\pi^-+{}^6\text{Li}\rightarrow 2{}^3\text{H}$	$\pi^-+{}^7\text{Li}\rightarrow{}^3\text{H}+{}^4\text{H}$	$\pi^-+{}^7\text{Li}\rightarrow{}^3\text{H}+{}^4\text{H}^*$
Branching ratio	$(3.4\pm0.5)\times10^{-4}$	$(3.7\pm1)\times10^{-4}$	$(4\pm1)\times10^{-4}$

result of its proximity to the peak associated with the two-triton breakup of ^{6}Li (Fig. 5), we know the ground-state energy accurately enough to conclude that the first level of ^{4}H is a p state[15] and that it is highly polarized along the direction of the ^{4}H momentum. The χ^2 associated with the statistical fits using various values of ^{4}H mass and width are shown in Table II. The widths associated with the best fits to the angular distribution are in reasonable agreement with those obtained from the widths of the range peaks.

A similar statistical procedure for the second level of ^{4}H showed that an isotropic decay distribution resulted in an acceptable fit to the data. A $\cos^2\theta$ decay distribution seems to be entirely unacceptable. The quality of the least-squares fits for this level are given in Table III.

There is some evidence for an additional enhancement in the first part of the chamber. In particular, the range curve associated with events whose opening angle was between 0.125 and 0.225 rad (Fig. 8) appears to indicate a shoulder on the high-mass side of the peak corresponding to the second level. As discussed earlier, a third Gaussian was included to fit the data in this part of the chamber. The angular distribution corresponding to this third Gaussian can be fitted adequately, assuming isotropic decay of H^4, a Q value of 12.3 MeV, and a width of 4 MeV. We think, however, that this level requires further experimental confirmation, since it lies near the first few gaps of our range chamber, where the statistical significance is lower because (a) the first two gaps are outside the overlap region of our two sets of data and (b) the correction for the angle of traversal through the absorber is somewhat uncertain.

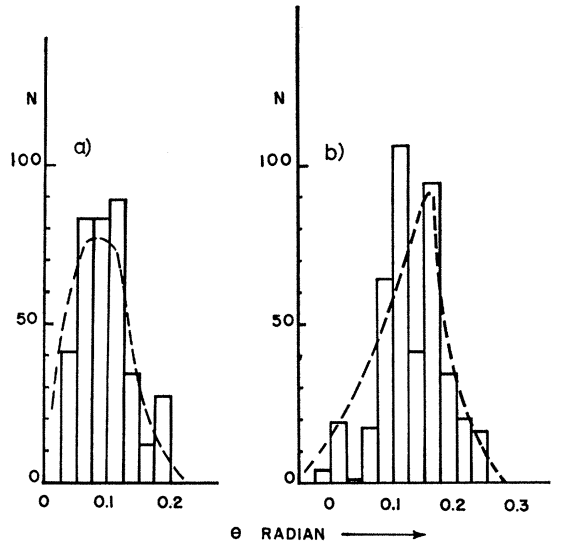

FIG. 9. (a) Angular distribution of the areas under the first Gaussian fitted to Fig. 8. The curve shows the best fit obtained with a $\cos^2\theta$ distribution in the c.m. system of the ^{4}H. The parameters of the best fit are $Q=3.2$ MeV, $\Gamma=3$ MeV, $\chi^2=6$. (b) Angular distribution of the areas under the second Gaussian fitted to Fig. 8. The curve shows the best fit obtained with an isotropic c.m. distribution. The parameters of the best fit are $Q=7.1$ MeV, $\Gamma=2.5$ MeV, $\chi^2=16$. Note that the Q values differ slightly from the ones obtained from the inherently more accurate range distribution. It is these latter Q values that we wish to quote for the energy of the ^{4}H levels.

[15] This is, of course, to be expected from the Pauli principle.

BRANCHING RATIOS

Eventually it may be possible to develop a theory that will relate the probability of the pion-induced fission modes to the existence of multinucleon clusters in the nucleus. Therefore the branching ratios for these processes are of interest. Since all stopping pions undergo nuclear capture, we obtained the branching ratio of a reaction by dividing the number of events due to this reaction by the total number of pion stops, correcting for the solid angle. The number of stops could be related to the number of $123\bar{4}$ counts by taking the difference between $123\bar{4}$ rates with the target in and with the target out for a fixed number of 12 counts. Within our experimental uncertainty the branching ratio obtained in this way for the two-triton breakup of Li^6 agreed with a more precise measurement made in a later run.[16] The branching ratios for the H^4 levels have therefore been normalized to that new measurement.

The solid angle was taken to be that of the range-chamber side, with a small correction, for the finite size of counter 7. As discussed earlier, the dependence of solid angle on range-chamber penetration depth was also included. The results are given in Table IV.

SEARCH FOR ^{5}H

In a separate run with a natural Li target the amount of absorber behind counter 6 was increased to the point where deuterons from the hypothetical reaction

$$\pi^-+{}^7\text{Li}\rightarrow{}^2\text{H}+{}^5\text{H} \qquad (5)$$

would have stopped in the range chamber. These deuterons have an energy between 72 and 78 MeV, depending on the Q value of the reaction $^5\text{H}\rightarrow{}^3\text{H}+2n$.

[16] R. C. Minehart, L. Coulson, W. Grubb, III, and K. Ziock, following paper, Phys. Rev. **177**, 1464 (1969).

Because of the relatively small specific energy loss of the deuterons this energy interval translates into a range interval exceeding the thickness of our range chamber. For this reason three sets of data were taken with 200, 250, and 300 mil of aluminum absorber in front of the range chamber. The total number of stopping pions was the same (5.4×10^7) for each of these sets. The three sets were corrected for the angle of traversal (range correction) and were superimposed in the manner discussed above. The resulting 30-bin range curve for events with $\theta<0.25$ rad is shown in Fig. 10.

If the ^{5}H decays to ^{3}H+$2n$ with a Q value less than 3 MeV, the opening angle for the triton is less than 0.25 rad. Shown in Fig. 10 is the peak that one would expect if ^{5}H with a Q value of 3 MeV and a width of $\Gamma=3$ MeV were formed with a branching ratio of $B=7\times10^{-5}$. This branching ratio corresponds to a peak height equal to three times the statistical uncertainty in the background. At larger Q values the opening angle increases, so that the background increases, thereby increasing the upper limit on the branching ratio. For wider levels and for several unresolved levels the upper limit set by our data also increases. These effects have been studied with Monte Carlo calculations, assuming a combination of a background whose shape is given by our data and a peak with varying position and width. From these calculations we have estimated upper limits for the branching ratio as shown in Table V.

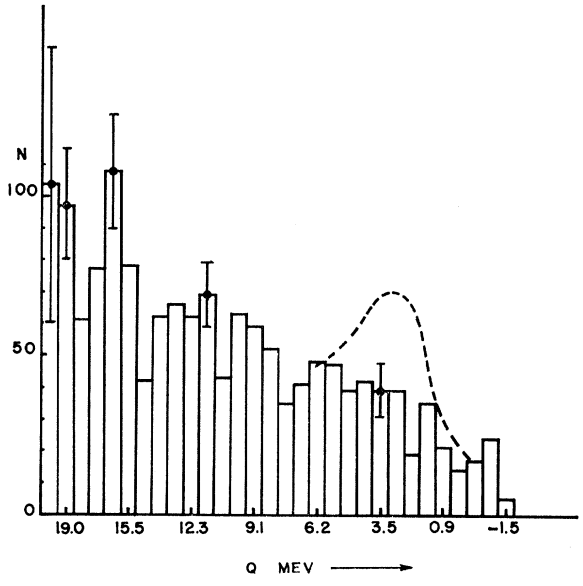

FIG. 10. Range curve for particle pairs with an opening angle $\theta<0.25$ rad (θ measures the deviation from collinearity). The dotted line shows the peak expected if ^{5}H were formed with $Q=3$ MeV, $\Gamma=3$ MeV, and a branching ratio $B=7\times10^{-5}$.

TABLE V. Upper limits for the branching ratio for the formation of ^{5}H for various assumed Q values and level widths.

Q (MeV)	$\Gamma=3$ MeV	$\Gamma=6$ MeV	$\Gamma=0$
<0			7×10^{-6}
3	7×10^{-5}	2×10^{-4}	
8	10^{-4}	2×10^{-4}	

If ^{5}H is assumed to be particle-stable, we can set a more stringent limit on the branching ratio. Stable ^{5}H must be collinear with the deuteron produced in reaction (5). If we sum all events with an angle $\theta<0.025$ rad for which one particle has a range corresponding to $Q<0$, we obtain a branching ratio $B<10^{-5}$.

These results confirm the earlier though less rigorous upper limit set by Cohen *et al.*[6]

SUMMARY AND CONCLUSIONS

Negative-pion capture in ^{6}Li and ^{7}Li can lead to fission into two hydrogen nuclei. The reactions observed in this experiment were

$$\pi^-+{}^6\mathrm{Li}\rightarrow 2{}^3\mathrm{H},$$

$$\pi^-+{}^7\mathrm{Li}\rightarrow {}^3\mathrm{H}+{}^4\mathrm{H},$$

$$\pi^-+{}^7\mathrm{Li}\rightarrow {}^3\mathrm{H}+{}^4\mathrm{H}^*.$$

The branching ratios for these processes as given in Table IV are all of the same order of magnitude and are small compared to the predominant mode of two-nucleon emission. The lifetimes of the two observed particle-unstable states of ^{4}H, as obtained from the level widths, are

$$(2.2\pm0.7)\times10^{-22}\ \text{sec}$$

and

$$(1.9\pm0.7)\times10^{-22}\ \text{sec},$$

respectively, for the ground state and the first excited state. We have also searched for the reaction

$$\pi^-+{}^7\mathrm{Li}\rightarrow {}^2\mathrm{H}+{}^5\mathrm{H}$$

and have established an upper limit on its branching ratio.

ACKNOWLEDGMENTS

We thank P. J. Castleberry for his help during some of the runs and W. Stephens for the design and construction of much of the electronic equipment used in the experiment. We also wish to express our gratitude for the cooperation and hospitality of the staff of the Space Radiation Effects Laboratory.